RSC Advances

ROYAL SOCIETY OF CHEMISTRY

www.rsc.org/advances

Journal Name

RSCPublishing

ARTICLE

An enzyme-responsive supra-amphiphile constructed by pillar[5]arene/acetylcholine molecular recognition

Cite this: DOI: 10.1039/xoxxoooooox

Guocan Yu,* Jie Yang, Danyu Xia and Yong Yao

Received ooth 2014,
Accepted ooth 2014

DOI: 10.1039/xoxxoooooox

www.rsc.org/

A novel molecular recognition motif between a water-soluble pillar[5]arene (**WP5**) and acetylcholine is established with an association constant of $(5.05 \pm 0.13) \times 10^4$ M^{-1}. Based on this molecular recognition motif, an enzyme-responsive supra-amphiphile is constructed by introducing an amphiphilic guest (**PyCh**) that is sensitive to acetylcholinesterase. Furthermore, supramolecular hybrid materials are prepared by introducing golden nanoparticles (AuNPs) into these supramolecular systems, which show enzyme-responsive catalytic abilities for the borohydride reduction of 4-nitroaniline.

Introduction

Supra-amphiphiles[1] are amphiphiles that are linked by noncovalent interactions, such as π-π stacking interactions, hydrogen bonding, charge-transfer interactions, and electrostatic interactions.[2] Because supra-amphiphiles are synthesized through noncovalent interactions, the need for time-consuming organic synthesis can be greatly reduced. Furthermore, functional supramolecular nanostructures can be easily constructed by introducing building blocks with stimuli-responsive functional moieties into the supra-amphiphiles. Numerous external stimuli such as temperature change, pH-change, redox, and light have been utilized in the construction of stimuli-responsive self-assembly systems.[3] Among them, enzyme-responsive self-assembly is especially attractive on account of its good biocompatibility and sensitivity, and therefore displays potential applications in biological materials and drug delivery systems.[4] Enzymes play significant roles in a series of biochemical processes and aberrations in the enzyme expression level often cause many diseases. Acetylcholine (ACh), one of many neurotransmitters in the autonomic nervous system, has functions both in peripheral nervous system and central nervous system, and is the only neurotransmitter used in the motor division of the somatic nervous system.[5] Damage to the cholinergic (acetylcholine-producing) system in the brain has been shown to be plausibly associated with Alzheimer's disease.[5a,b] Moreover, in cardiac tissue acetylcholine neurotransmission has an inhibitory effect, lowering heart rate. Consequently, the construction of a supra-amphiphile which can be responsive to cholinesterases, such as acetylcholinesterase (AChE), is of particular interest and importance not only in fundamental research but also in practical application to biotechnology and medicine, because only a limited amount of endeavour has been devoted so far to this research area.

Pillar[*n*]arenes, mainly including pillar[5]arenes[6] and pillar[6]arenes,[7] are a new kind of macrocyclic hosts, next to crown ethers, cyclodextrins, calixarenes, and cucurbiturils.[8,9] Compared with the basket-shaped structure of *meta*-bridged calixarenes, pillar[*n*]arenes are linked by methylene (-CH_2-) bridges at *para*-positions of 2,5-dialkoxybenzene rings, forming a unique rigid pillar architecture. The unique symmetrical structure and easy functionalization of pillararenes have afforded them superior properties in host–guest recognition. Pillararenes act as useful platforms for the construction of various interesting supramolecular systems, including liquid crystals,[7g] cyclic dimers,[10] chemosensors,[11] supramolecular polymers,[12] drug delivery systems,[13] transmembrane channels[14] and cell glue.[15] A series of external stimuli, such as temperature change,[16a,d] light,[16b] pH-change[16c] and redox,[16e] have been utilized to develop sophisticated pillararene-based supramolecular systems which were employed in various fields. However, enzyme-responsive pillararene-based self-assembly has not been reported up to now.

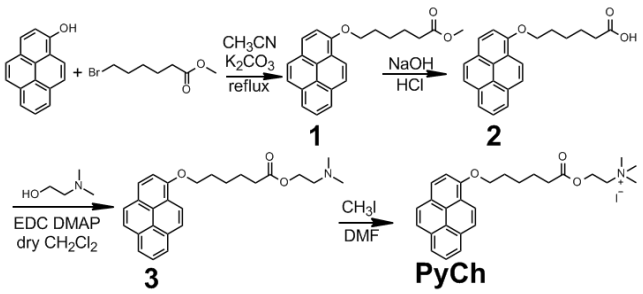

Scheme 1. Synthetic route to **PyCh**.

Considering that the preparation of self-assemblies possessing novel stimuli-responsiveness is extremely important for the potential application in a broad range of fields, such as memory storage, smart supramolecular polymers, drug delivery systems, sensors, protein probes, and functional nanodevices,[17] we are interested in the construction of enzyme-responsive pillararene-based supra-amphiphiles to obtain functional supramolecular systems. Herein, we designed and fabricated an enzyme-responsive supra-amphiphile comprised of a water-soluble pillar[5]arene (**WP5**) and an amphiphilic guest (**PyCh**) with choline as the hydrophilic part and pyrene derivative as the hydrophobic section. Guest **PyCh** itself self-assembled in water to form nanosheets driven by π-π stacking interactions between the pyrenyl groups. Upon addition of **WP5**, the nanosheets transformed into nanoparticles due to steric hindrance and electrostatic repulsion generated upon insertion of the anionic

hosts. Because of the enzyme-responsiveness of **PyCh**, both the nanosheets formed by **PyCh** and the nanoparticles formed by the host–guest complex **WP5⊃PyCh** changed into nanoribbons in the presence of AChE. Considering the existence of trimethylammonium groups on the surfaces of nanosheets and negative carboxylate anions on the surfaces of nanoparticles, these self-assemblies were further employed to prepare supramolecular hybrid materials by fabrication with gold nanoparticles (AuNPs), which were utilized as catalysts for the borohydride reduction of 4-nitroaniline.

Fig. 1 Structural illustration of the building blocks (**WP5**, **PyCh** and acetylcholine) and schematic representation of the resulting enzyme-responsive self-assembly.

Results and discussion

Host–guest interactions molecular recognition between pillar[5]arene and acetylcholine. The host–guest interactions between **WP5** and **PyCh** were firstly studied by ^{1}H NMR spectroscopy by using acetylcholine iodide (**M**) as a model compound due to the relatively poor solubility of **PyCh**. Compared with the spectrum of free **M** (a in Fig. 2a), the resonance peaks related to protons H^1, H^2, H^3 and H^4 of **M** displayed substantial upfield shifts ($\Delta\delta$ = −0.14, −0.31, −0.24 and −0.14 ppm for H^1, H^2, H^3 and H^4, respectively) in the presence of an equivalent amount of **WP5** (c in Fig. 2a). The reason was that these protons were shielded by the electron-rich cyclic structure upon forming a threaded structure between **WP5** and **M**. Moreover, extensive broadening effects were observed for the peaks corresponding to protons on **M** due to complexation dynamics.[16b] On the other hand, the protons on **WP5** also exhibited slight chemical shift changes due to the interactions between **WP5** and **M**. The resonance peaks related to protons H^b on the benzene rings and H^c on the methylene bridges shifted downfield ($\Delta\delta$ = 0.04 and −0.03 ppm for H^b and H^c, respectively). From our previous work, we knew that the cavity of pillar[5]arene could only encapsulate four methylenes.[6b] Therefore, we speculated that the ester and methyl groups were situated in the cavity of **WP5**, while the methylenes and trimethylammonium group resided on the rim of **WP5** due to the electrostatic interactions between the carboxylate anions on the host and the trimethylammonium cation on the guest.

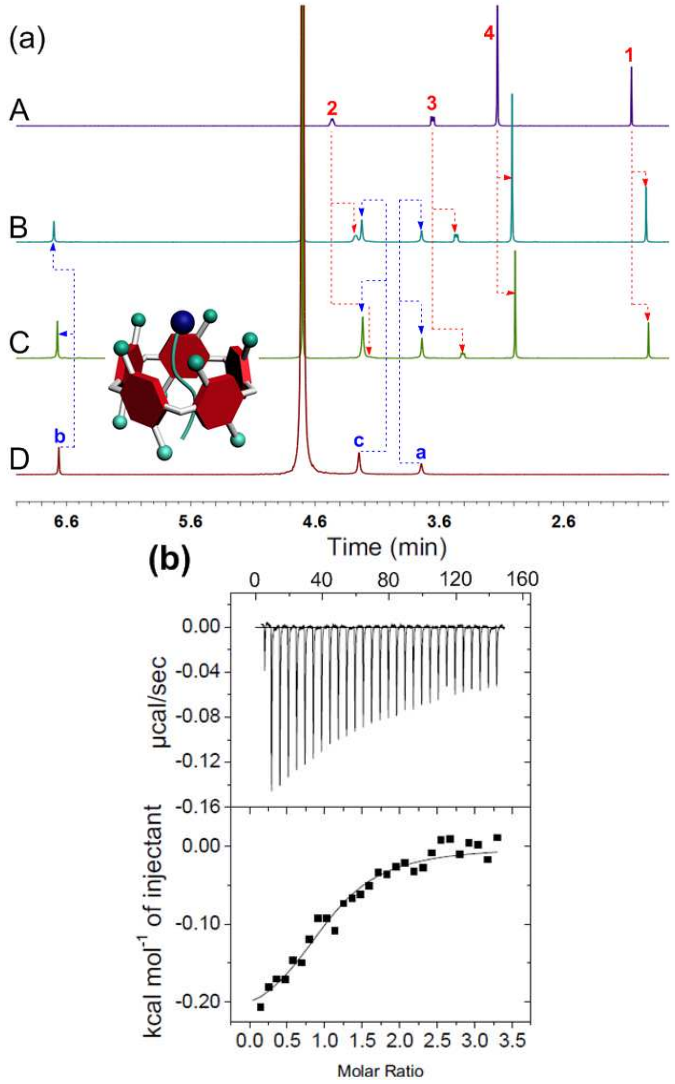

Fig. 2 (a) Partial ^{1}H NMR spectra (400 MHz, D_2O, 295 K): A. **M** (2.00 mM); B. **WP5** (2.00 mM) and **M** (6.00 mM); C. **WP5** (2.00 mM) and **M** (2.00 mM); D. **WP5** (2.00 mM). (b) Microcalorimetric titration of **M** with **WP5** in water at 298.15 K. Top: raw ITC data for 29 sequential injections (10 μL per injection) of an **M** solution (2.00 mM) into a **WP5** solution (0.100 mM); Bottom: net reaction heat obtained from the integration of the calorimetric traces.

2D NOESY NMR spectroscopy is a useful tool to study the relative positions of the components in host−guest inclusion complexes. It was used to investigate the complexation between **WP5** and **M**. A nuclear Overhauser effect (NOE) correlation was observed between the signals related to protons H^1 on **M** and protons H^b on **WP5** (Fig. S13), while no NOE was observed between protons H^2, H^3 and H^4 on **M** and protons on **WP5**, suggesting that protons H^1 were located in the cavity of **WP5**. To provide further evidence for the host−guest interactions between **WP5** and **M** and to obtain insight into the binding geometry in complex **WP5⊃M**, molecular modeling was performed (Fig. S15). The molecular

geometry optimization of **WP5⊃M** shows that the guest is tightly wrapped within **WP5**. Noticeably, the cationic segment of **M** is located on the upper side of **WP5** to successfully achieve multivalent electrostatic interactions with carboxylate groups on **WP5**, and the tail of **M** containing ester and methyl groups locates inside the cavity of **WP5**. The results obtained from 2D NOESY NMR spectroscopy and molecular modelling were in good agreement with our speculation mentioned above.

Isothermal titration calorimetry (ITC) experiments were performed to provide thermodynamic insight into the inclusion complexation between **WP5** and **M**. From Fig. 2b and Fig. S14, the K_a value of **WP5⊃M** was determined to be $(5.05 \pm 0.13) \times 10^4$ M^{-1} in 1:1 complexation. The binding affinity of this host−guest system can be attributed to the cooperativity of multiple electrostatic interactions between the carboxylate anionic groups on the rigid pillar[5]arene receptor platform and the cationic trimethylammonium part and hydrophobic interactions between the alkyl chain and the host. Furthermore, the enthalpy and entropy changes were obtained ($\Delta H° < 0$; $T\Delta S°>0$; $|\Delta H°| < |T\Delta S°|$), indicating that this complexation was primarily driven by the entropy change with enthalpic assistance (Fig. S14).

Enzyme-responsive self-assembly of the supra-amphiphile. After the establishment of the pillar[5]arene/acetylcholine recognition motif in water, we applied it to construct an enzyme-responsive supra-amphiphile and studied the controllable self-assembly of this supra-amphiphile. The self-assembly of amphiphilic **PyCh** in water was investigated first. From Fig. S18, the critical aggregation concentration (CAC) of **PyCh** was determined to be 1.25×10^{-6} M using the concentration-dependent conductivity. Transmission electron microscopy (TEM) experiments assisted in the visualization of the self-assembly nanostructure of **PyCh**. As shown in Fig. 3a, two-dimensional nanosheets were observed clearly with very thin thickness. Fluorescence microscopy (Fig. 3d) and scanning electron microscopy (SEM) were further utilized to confirm the morphology of the self-assemlies formed by **PyCh**, coinciding with the results obtained from TEM. The thickness of the nanosheets was calculated to be about 5 nm (Fig. 3h and Fig. S23c). Notably, the extended length of **PyCh** is ~2.3 nm, close to half the thickness of the nanosheets, indicating a bilayer packing mode of **PyCh** in the nanosheets (Fig. 1). The packing pattern of **PyCh** in the nanosheets was studied by UV-vis spectroscopy and X-ray diffraction (XRD). An increase in the concentration caused a blue shift (Fig. S22), which indicated an *H*-aggregation form, suggesting that adjacent pyrene aromatic rings underwent considerable overlap through π-π stacking interactions (Fig. 1).[16c] Moreover, the bilayer structure of the membrane was confirmed by XRD. As shown in Fig. S21a, the thickness of the bilayer was calculated to be 4.5 nm, close to the length of two **PyCh** molecules with antiparallel packing and overlapped pyrene rings (Fig. 1),[18a] in accordance with the results obtained from TEM and SEM images.

Interestingly, the critical aggregation concentration of **PyCh** in the presence of an equivalent amount of **WP5** increased to 1.52×10^{-4} M (Fig. S19). The CAC value of **PyCh** was enhanced pronouncedly by a factor of *ca.* 122 due to its host−guest complexation with **WP5**. Moreover, the resultant self-assemblies changed from nanosheets to nanoparticles with an average diameter of about 250 nm (Fig. 3b). SEM also provided convincing insight into the transformation from nanosheets for **PyCh** to nanoparticles for **WP5⊃PyCh** (Fig. 3g−i). Dynamic light scattering (DLS) was further empolyed to confirm the size of the aggregrates formed by **WP5⊃PyCh**. As shown in Fig. S20, the main diameter distribution of the aggregates was around 263 nm, which was in harmony with the corresponding TEM and SEM images. It should be pointed out that the diameter of the nano-aggregates measured by DLS was little larger than that obtained in TEM images, attributed to the swelling effect of the spherical structures in water.[7d]

A mechanism was proposed to explain the morphological transformation from nanosheets for **PyCh** to nanoparticles for **WP5⊃PyCh** (Fig. 1). The self-assembled structure of the aggregates, formed by the two distinct bilayers, is determined by the curvature of the membrane.[18] For **PyCh** alone, highly directional π-π stacking interactions between the pyrene aromatic rings are achieved in water, thus leading to the formation of 2D self-assembly in a bilayer structure. The size of trimethylammonium cation group is smaller than the cavity of **WP5**,[6b] so the anionic hosts insert into the membrane of the nanosheets and form 1:1 [2]pseudorotaxanes upon complexation with **WP5**. Due to the existence of steric hindrance and electrostatic repulsion generated upon the insertion of **WP5**, the membrane curvature of the nanosheets become higher, resulting in the formation of nanoparticles with a spherical structure.[18]

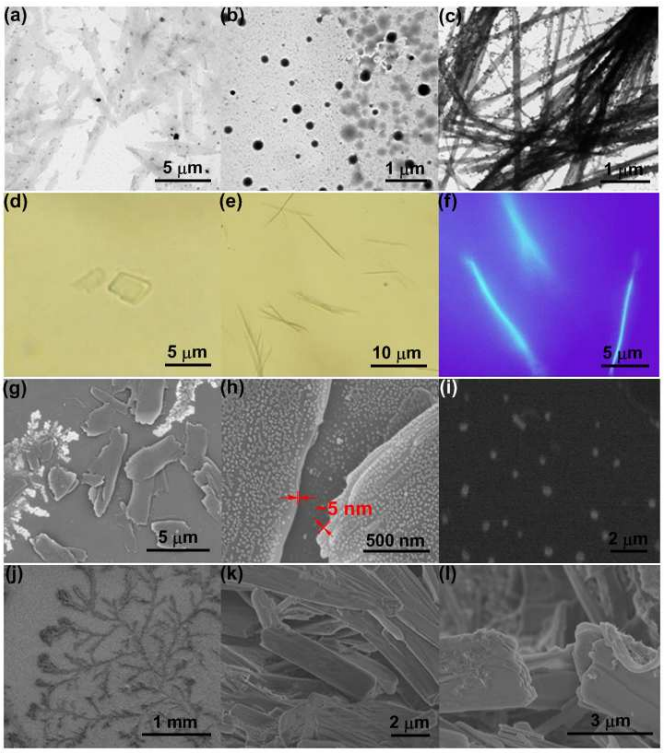

Fig. 3 TEM images: (a) **PyCh**; (b) **WP5⊃PyCh**; (c) **WP5⊃PyCh** treated with AChE. Bright field images: (d) **PyCh**; (e) **WP5⊃PyCh** treated with AChE. (f) Fluorescence microscopic image of **WP5⊃PyCh** treated with AChE. SEM images: (g) **PyCh**; (h) enlarged image of (g); (i) **WP5⊃PyCh**; (j) **WP5⊃PyCh** treated with AChE; (k) enlarged image of (j); (l) enlarged image of a broken nanoribbon. The concentrations of **PyCh** and **WP5⊃PyCh** were higher than their corresponding CAC values. It should be noted that the samples were coated with golden nanoparticles in SEM experiments, and the particles on the nanosheets (Fig. 3h) were the golden nanoparticles.

PyCh contains an alkanoylcholine that can be hydrolyzed to the corresponding acid (**PyH**) and choline by cholinesterases (Fig. 1), thereby affecting the morphologies of the self-assemblies. Mass spectral measurements were performed to monitor the enzymatic cleavage of the ester bonds of **PyCh**. As shown by mass spectra of **PyCh** at different time points in the presence of AChE, the peak at 418.0 corresponding to $[\mathbf{PyCh} - I]^+$ weakened after 5 h (Fig. S25), and almost disappeared 12 h later (Fig. S26), in concert with the appearance of the peaks at 105.0 and 332.1 related to choline and

PyOH, respectively, indicating that almost all of the ester bonds were cleaved. Interestingly, the self-assembly structures of both **PyCh** and **WP5⊃PyCh** underwent dramatic changes as revealed by TEM in the presence of AChE. Nanoribbons several micrometers in length and 200–300 nm in width were observed by culturing the nanoparticles formed by **WP5⊃PyCh** with AChE at 37 °C. Notably, the coexistence of nanoparticles and nanoribbons was also observed (Fig. 3c and Fig. S23a), demonstrating the gradual transformation from nanoparticles to nanoribbons caused by the hydrolysis of **PyCh** in the presence of AChE. SEM images provided useful information about the morphological changes of the self-assemblies (Fig. 3j–l). Compared with the nanoparticles, dendritic aggregates with much larger size, several micrometers, were observed after the solution had stood for 2 weeks (Fig. 3j) in the presence of AChE. More exciting, we found that these dendritic superstructures were composed of nanoribbons in the plane-to-plane packing mode (Fig. 3k, l). The thickness of the nanoribbons was ~20 nm, as observed from a broken multiple-nanoribbon (Fig. 3l and Fig. S23d), indicating that the nanoribbons had a multi-layer structure. Similarly, the nanosheets formed by **PyCh** alone also changed into nanoribbons in the presence of AChE, as verified by TEM (Fig. S23b). We also knew that the bilayer structure was retained when the nanosheets transformed into nanoribbons through XRD data (Fig. S21b). It should be noted that the hydrolysis rate of the host–guest complex **WP5⊃PyCh** by AChE was much slower than that of free **PyCh** because there existed a dynamic equilibrium between the complexed and uncomplexed states of **PyCh**, and AChE attacks only the free species.[8r]

PyCh both in the nanosheets and in the nanoparticles was hydrolyzed into **PyH** and choline in the presence of AChE, and the amphiphilic **PyH** self-assembled in water through π-π stacking interactions. On the other hand, interlayer mutiple hydrogen bonds due to the existence of carboxylic acid groups on the surface of the nanoribbons caused the formation of multi-layer aggregates. However, the nanosheets self-assembled from **PyCh** did not pack together to generate larger aggregates owing to the presence of the cationic groups on the surface and the attendant electrostatic repulsion between the nanostructures. It should be pointed out that there was no interaction between **PyH** and **WP5**, so the morphologies of the self-assemblies obtained from hydrolysis of the nanosheets and from the nanoparticles were the same, whether or not **WP5** was present.

Prepation of Supramolecular Hybrid Materials and Application in Borohydride Reduction of 4-Nitroaniline. With the enzyme-responsive self-assemblies in hand, we explored possible applications of these novel supramolecular systems. Considering the existence of trimethylammonium groups on the surfaces of nanosheets and negative carboxylate anions on the surfaces of nanoparticles, these two self-assemblies could be employed to prepare supramolecular hybrid materials with gold nanoparticles.[19] Self-assembled organic aggregates have been demonstrated to be useful in the fabrication of metallized self-assemblies.[19b] By using the present nanosheets and nanoparticles as the templates, gold nanoparticles were directly loaded onto the surfaces of the self-assemblies at room temperature to form supramolecular hybrid materials (AuNPs@nanosheets and AuNPs@nanoparticles). As shown in TEM images (Fig. 4a–c), we found that the AuNPs adhered to the surface of the self-assemblies with an average diameter of about 6 nm (Fig. S27). As shown in UV–vis spectra (Fig. S28), the well-known surface plasmon resonance (SPR) of AuNPs around 520 nm was observed, suggesting the successful preparation of supramolecular hybrid materials. Moreover, Fourier transform IR spectroscopy (Fig. S29) and energy dispersive spectrometry (EDS) experiments (Fig. S30, S31) were conducted to confirm the successful preparation of supramolecular hybrid materials.[6j]

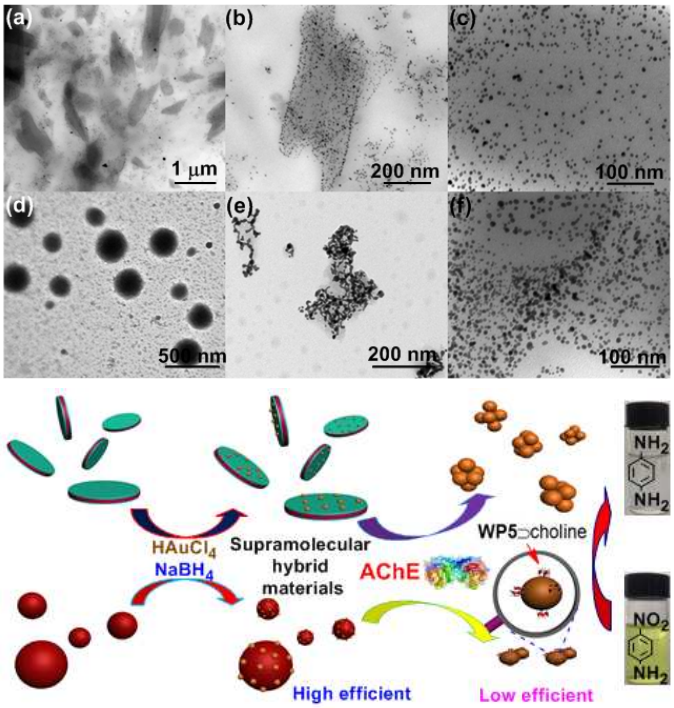

Fig. 4 TEM images: (a) AuNPs@nanosheets; (b) enlarged image of (a); (c) enlarged image of (a); (d) AuNPs@nanoparticles; (e) AuNPs@nanosheets treated with AChE; (f) AuNPs@nanoparticles treated with AChE. Cartoon illustration of the prepration of supramolecular hybrid materials and application in the reduction of 4-nitroaniline.

Naturally, these hybrids also displayed excellent enzyme responsivity due to the presence of **PyCh**. For the hybrids, the diameters of the AuNPs became larger and their shapes became smoother and rounder by treatment with AChE due to Ostwald ripening (Fig. 4e, f),[6j] because the total surface area can be minimized by the formation of spherical particles, and larger particles are more energetically favored than smaller particles. Furthermore, we applied TEM to characterize the aggregation process of AuNPs at the nanoscale before and after aggregation induced by AChE. A greater degree of aggregation was observed for the AuNPs corresponding to AuNPs@nanosheets after hydrolysis by AChE (Fig. 4f). The reasons were as follows: the choline was attached to the surface of AuNPs when **PyCh** in AuNPs@nanosheets hydrolyzed into **PyH** and choline, resulting in the growth of AuNPs into larger aggregates (Fig. 4b). However, for the AuNPs@nanoparticles, the choline derived from **PyCh** formed a stable host–guest complex with **WP5**. Owing to the presence of carboxylate anionic groups on the macrocyclic ring, the host–guest complex **WP5⊃**choline can be considered as a cluster of carboxylate groups and sodium, providing a shell of anions and cations around the gold nanoparticles, thus stabilizing them in aqueous solution. Therefore, relatively smaller changes in the size of AuNPs occurred for AuNPs@nanoparticles after the hydrolysis of **PyCh** (Fig. 3e).

The physical and chemical properties are closely related to the morphology and size of the nanomaterials. In our systems, the sizes of AuNPs in these supramolecular hybrids underwent significant changes after hydrolysis, naturally affecting their properties. As we know, one of the important applications of AuNPs is to catalyze reactions that are otherwise not feasible. Therefore, we examined the performance of these hybrids as catalysts for the borohydride

reduction of 4-nitroaniline as a model reaction. The peak at 400 nm corresponding to the characteristic absorption of 4-nitroaniline remained unaltered for a long time in the absence of AuNPs, indicating that the reducing agent NaBH4 itself was unable to reduce 4-nitroaniline.[16a] On the contrary, the absorption band at 400 nm decreased gradually with the concomitant appearance of new peaks at 300 nm and 240 nm upon addition of the supramolecular hybrids (AuNPs@nanosheets or AuNPs@nanoparticles) into the reaction system, indicating that 1,4-diaminobenzene was produced (Fig. S32, 31), accompanied by a color change from yellow to transparent (Fig. 4). The kinetic reaction rate constants for the reduction with AuNPs@nanosheets and AuNPs@nanoparticles were estimated to be $(1.85 \pm 0.15) \times 10^{-3}$ s^{-1} and $(2.61 \pm 0.28) \times 10^{-3}$ s^{-1}, respectively. Notably, the kinetic reaction rate constant of AuNPs@nanoparticles decreased to $(1.78 \pm 0.11) \times 10^{-3}$ s^{-1} after treatment with AChE for 12 h (Fig. S34), which was higher than that of AuNPs@nanosheets after the same treatment ($(1.01 \pm 0.09) \times 10^{-3}$ s^{-1}, Fig. S35). The reasons was that the catalytic activity of the AuNPs is possibly through electron transfer from the BH_4^- anion to nitro compounds mediated by the large Fermi level shift of the nanoparticles.19a Compared with the AuNPs@nanosheets and AuNPs@nanoparticles, the sizes of AuNPs became larger due to the hydrolysis of **PyCh** by the AChE, resulting in the reduction of their specific surface area. For the AuNPs@nanoparticles, the hydrolyzate **WP5**⊃choline could act as clusters to protect AuNPs from aggregating to some extent, so the corresponding kinetic reaction rate was relatively larger.

Conclusions

In summary, a new pillar[5]arene/acetylcholine molecular recognition motif was established. Based on this molecular recognition motif, an enzyme-responsive supra-amphiphile was constructed by introducing an amphiphilic guest **PyCh**, which was sensitive to enzyme AChE. In contrast to the nanosheets self-assembled by **PyCh** alone through π-π stacking interactions between the pyrenyl groups, the host–guest complex **WP5**⊃**PyCh** self-assembled into nanoparticles induced by a curvature-dependent mechanism. **PyCh** was hydrolyzed into **PyH** and choline in the presence of AChE, resulting in the transformation of the nanosheets and nanoparticles into multi-layer nanoribbons. Intermolecular hydrogen bonds between the carboxylic acid groups on the surfaces of the nanoribbons played a significant role in the generation of these aggregates. Due to the existence of trimethylammonium groups on the surfaces of the nanosheets and negative carboxylate anions on the surfaces of the nanoparticles, supramolecualr hybrid materials were prepared by introducing golden nanoparticles (AuNPs). Furthermore, these hybrids exhibited excellent catalytic abilities for the borohydride reduction of 4-nitroaniline as a model reaction. The specific surface areas of AuNPs in these supramolecular hybrids underwent significant changes after hydrolysis due to the growth of the AuNPs, resulting in the reduction of their catalytic abilities. These results exemplify the enormous potential of enzyme-responsive self-assembly for the construction of well-defined nanostructures that can be applied in many fields, including supramolecular polymers, nanoelectronics, and sensors.

Experimental

Synthesis of 1. Methyl 6-bromohexanoate (5.16 g, 20.0 mmol) and K_2CO_3 (6.62 g, 48.0 mmol) were added to a solution of 1-pyrenol (2.18 g, 10.0 mmol) in CH_3CN (100 mL). The mixture was heated in a three-necked flask under nitrogen atmosphere at reflux for 24 h. The cooled reaction mixture was filtered and washed with chloroform. The filtrate was evaporated under vacuum, and the residue was purified by flash column chromatography on silica gel (dichloromethane/petroleum ether = 1:5, *v*/*v*) to afford 1 as a white solid (3.54 g, 83%), mp 112.5−113.8 °C. The proton NMR spectrum of **1** is shown in Fig. S1. ^{1}H NMR (400 MHz, chloroform-*d*, room temperature) δ (ppm): 8.45 (d, J = 8.0 Hz, 1H), 8.09 (t, J = 8.0 Hz, 3H), 8.01 (d, J = 8.0 Hz, 1H), 7.96–7.03 (m, 2H), 7.87 (d, J = 8.0 Hz, 1H), 7.51 (d, J = 8.0 Hz, 1H), 4.31 (t, J = 8.0 Hz, 2H), 3.68 (s, 3H), 2.40 (t, J = 8.0 Hz, 2H), 2.02–1.99 (m, 2H), 1.84–1.76 (m, 2H), 1.71–1.63 (m, 2H). The ^{13}C NMR spectrum of **1** is shown in Fig. S2. 13C NMR (125 MHz, chloroform-*d*, room temperature) δ (ppm): 174.11, 153.11, 131.76, 131.71, 127.26, 126.32, 126.08, 125.86, 125.49, 125.19, 124.99, 124.94, 124.22, 124.12, 121.24, 120.42, 109.12, 68.61, 51.55, 34.06, 29.21, 25.91, 24.80. LRESIMS is shown in Fig. S3: *m*/*z* 346.9 $[M + H]^+$ (100%). HRESIMS: *m*/*z* calcd for $[M + H]^+$ $C_{23}H_{23}O_3$, 347.1647, found 347.1655, error 2 ppm.

Synthesis of 2. A solution of **1** (3.46 g, 10.0 mmol) in CH_3CH_2OH (40 mL) was treated with 40% aqueous sodium hydroxide (80 mL) at reflux for 12 h. The mixture was concentrated under reduced pressure, diluted with water (10 mL), and acidified with HCl. The precipitated product **2** was collected by filtration, washed with water and dried under vacuum as a white solid (3.09 g, 93%), mp 126.8−128.3 °C. The proton NMR spectrum of **2** is shown in Fig. S4. ^{1}H NMR (400 MHz, DMSO-d_6, room temperature) δ (ppm): 12.09 (s, 1H), 8.37 (d, J = 8.0 Hz, 1H), 8.24 (d, J = 8.0 Hz, 1H), 8.18 (t, J = 4.0 Hz, 2H), 8.13 (d, J = 8.0 Hz, 1H), 8.06 (t, J = 8.0 Hz, 2H), 8.01 (d, J = 8.0 Hz, 1H), 7.96 (d, J = 8.0 Hz, 1H), 7.75 (d, J = 8.0 Hz, 1H), 4.35 (t, J = 8.0 Hz, 2H), 2.29 (t, J = 8.0 Hz, 2H), 1.97–1.92 (m, 2H), 1.68–1.58 (m, 4H). The ^{13}C NMR spectrum of **2** is shown in Fig. S5. ^{13}C NMR (100 MHz, DMSO-d_6, room temperature) δ (ppm): 174.53, 152.67, 131.22, 131.08, 127.29, 126.37, 126.26, 126.00, 124.92, 124.62, 124.46, 124.30, 124.14, 124.09, 120.83, 119.33, 109.79, 68.37, 33.79, 28.63, 25.35, 24.39. LRESIMS is shown in Fig. S6: *m*/*z* 330.9 $[M - H]^-$ (100%). HRESIMS: *m*/*z* calcd for $[M - H]^-$ $C_{22}H_{19}O_3$, 331.1334, found 331.1341, error 2 ppm.

Synthesis of 3. To a solution of **2** (1.66 g, 5.00 mmol) and *N,N′*-dimethylethanolamine (1.78 g, 20.0 mmol) in dry CH_2Cl_2 (100 mL), 4-dimethylaminopyridine (DMAP, catalytic amount) and 1-(3'-dimethylaminopropyl)-3-ethylcarbodiimide hydrochloride (EDC, 1.79 g, 10.0 mmol) were added under nitrogen atmosphere. The mixture was stirred overnight at room temperature. The solution was evaporated under vacuum and the residue was purified by flash column chromatography on silica gel (dichloromethane/petroleum ether = 2:1, *v*/*v*) to afford **3** as a white solid (1.57 g, 78%), mp 104.1−106.4 °C. The proton NMR spectrum of **3** is shown in Fig. S7. ^{1}H NMR (400 MHz, chloroform-*d*, room temperature) δ (ppm): 8.45 (d, J = 8.0 Hz, 1H), 8.09 (t, J = 8.0 Hz, 2H), 8.03 (d, J = 8.0 Hz, 1H), 7.95–7.93 (m, 2H), 7.87 (d, J = 8.0 Hz, 1H), 7.51 (d, J = 8.0 Hz, 1H), 4,31 (t, J = 8.0 Hz, 2H), 4,31 (t, J = 8.0 Hz, 2H), 3.71 (t, J = 8.0 Hz, 2H), 2.55 (t, J = 8.0 Hz, 2H), 2.43 (t, J = 8.0 Hz, 2H), 2.26 (s, 6H), 1.84–1.64 (m, 6H). The ^{13}C NMR spectrum of *3* is shown in Fig. S7. ^{13}C NMR (100 MHz, chloroform-d, room temperature) δ (ppm): 173.75, 153.11, 131.76, 131.71, 127.26, 126.32, 126.07, 125.85, 125.49, 125.18, 124.98, 124.21, 124.12, 121.25, 120.41, 109.12, 68.62, 57.81, 45.67, 34.21, 29.22, 25.89, 24.76, 18.43. LRESIMS is shown in Fig. S9: *m*/*z* 404.0 $[M + H]^+$ (100%). HRESIMS: *m*/*z* calcd for $[M + H]^+$ $C_{26}H_{30}NO_3$, 404.2226, found 404.2214, error –3 ppm.

Synthesis of PyCh. A mixture of compound **3** (2.02 g, 5.00 mmol) and CH_3I (5.68 g, 40.0 mmol) was heated in *N,N′*-dimethylformamide (50 mL) at 50 °C for 12 h. The solvent was evaporated, and the residue was washed with CH_2Cl_2 to give **PyCh** as a light yellow solid (1.66 g, 61%), mp 116.4−118.1 °C. The proton NMR spectrum of **PyCh** is shown in Fig. S10. ^{1}H NMR (400 MHz, DMSO-d_6, room temperature) δ (ppm): 8.38 (d, J = 8.0 Hz,

1H), 8.25 (d, J = 8.0 Hz, 2H), 8.20 (t, J = 8.0 Hz, 2H), 8.14 (d, J = 8.0 Hz, 1H), 8.08 (d, J = 8.0 Hz, 1H), 8.03 (t, J = 8.0 Hz, 1H), 7.97 (d, J = 8.0 Hz, 1H), 7.76 (d, J = 8.0 Hz, 1H), 4.48–4.46 (m, 2H), 4,37 (t, J = 8.0 Hz, 2H), 3.67–3.65 (m, 2H), 2.45 (t, J = 8.0 Hz, 2H), 2.00–1.93 (m, 2H), 1.76–1.67 (m, 2H), 1.65–1.60 (m, 2H). The 13C NMR spectrum of **PyCh** is shown in Fig. S11. ^{13}C NMR (100 MHz, DMSO-d_6, room temperature) δ (ppm): 172.32, 152.62, 131.22, 131.06, 127.28, 126.41, 126.27, 126.01, 124.93, 124.66, 124.49, 124.36, 124.11, 120.78, 119.32, 109.79, 68.30, 63.72, 57.69, 54.90, 52.90, 33.32, 28.55, 25.23, 24.01. LRESIMS is shown in Fig. S12: m/z 418.0 $[M - I]^+$ (100%). HRESIMS: m/z calcd for $[M - I]^+$ $C_{27}H_{32}NO_3$, 418.2382, found 418.2393, error 3 ppm.

Critical Aggregation Concentration (CAC) Determination. Some parameters such as the conductivity, osmotic pressure, fluorescence intensity and surface tension of the solution change sharply around the critical aggregation concentration. The dependence of the solution conductivity on the solution concentration is used to determine the critical aggregation concentration. Typically, the slope of the change in conductivity versus the concentration below CAC is steeper than the slope above the CAC. Therefore, the junction of the conductivity-concentration plot represents the CAC value. To measure the CAC value of **PyCh** (or **WP5⊃PyCh**), the conductivities of the solutions at different concentrations were determined. By plotting the conductivity versus the concentration, we estimated the CAC value of **PyCh** (or **WP5⊃PyCh)**.

Preparation of Supramolecular Hybrid Materials. In a typical experiment, 0.10 mL of 1.0×10^{-4} M HAuCl4 and 6.0 mL of PyCh (or **WP5⊃PyCh**) aqueous solution were mixed in a 10 mL bottle. Then aqueous sodium borohydride (0.20 mL, 0.0125 g/mL) was injected into the above solution under vigorous stirring. The solution became wine red, indicating that supramolecular hybrid materials AuNPs@nanosheets and AuNPs@nanoparticles were immediately obtained.

Transmission Electron Microscopy (TEM) and Dynamic Light Scattering (DLS) Studies. The nanostructures of the self-assemblies were revealed using TEM. The concentrations of the solutions were higher than the corresponding critical aggregation concentrations of **PyCh** and **WP5⊃PyCh**. A solution of **PyCh** (or **WP5⊃PyCh**) was prepared first in water. TEM samples were prepared by drop-coating the solution on a carbon-coated copper grid. TEM experiments were performed on a HT-7700 instrument. The solution of **WP5⊃PyCh** was left to stand overnight and the insoluble precipitate was eliminated by using a microporous membrane before being used for DLS tests. The diameters of the assemblies were measured on a Nano-ZS ZEN3600 instrument.

Catalytic Reduction of 4-nitroaniline. The catalytic reduction of 4-nitroaniline was studied as follows. To a standard quartz cell with a 1-cm path length and about 4 mL volume, 3 mL of 0.20 mM 4-nitroaniline and 0.03 g of $NaBH_4$ (large excess) were added. Then the addition of supramolecular hybrids (0.04 mL) to the mixture caused a decrease in the intensity of the absorption of 4-nitroaniline. The absorption spectra were recorded in a scanning range of 200−700 nm at room temperature. The control experiment was also carried out in the absence of supramolecular hybrids.

Acknowledgements

This work was supported by the Fundamental Research Funds for the Central Universities.

Notes and references

Department of Chemistry, Zhejiang University, Hangzhou 310027, P. R. China. E-mail: guocanyu@zju.edu.cn

Electronic Supplementary Information (ESI) available: [Synthetic procedures, characterizations, and other materials]. See DOI: 10.1039/b000000x/

1 (a) K. Wang , D.-S. Guo, X. Wang and Y. Liu, *ACS Nano*, 2011, **5**, 2880–2894; (b) C. Wang, Z. Wang and X. Zhang, *Acc. Chem. Res.*, 2012, **45**, 608–618; (c) K. Wang , D.-S. Guo and Y. Liu, *Chem. Eur. J.*, 2012, **18**, 8758–8764.

2 (a) F. Huang, F. R. Fronczek and H. W. Gibson, *J. Am. Chem. Soc*., 2003, **125**, 9272–9273; (b) F. Huang, M. Lam, E. J. Mahan, A. L. Rheingold and H. W. Gibson, *Chem. Commun*., 2005, 3268–3270; (c) H.-B. Yang, N. Das, F. Huang, A. M. Hawkridge, D. C. Muddiman and P. J. Stang, *J. Am. Chem. Soc*., 2006, **128**, 10014–10015; (d) H.-B. Yang, K. Ghosh, B. H. Northrop, Y.-R. Zheng, M. M. Lyndon, D. C. Muddiman and P. J. Stang, *J. Am. Chem. Soc*., 2007, **129**, 14187–14189; (e) L. Chen, Y.-K. Tian, Y. Ding, Y.-J. Tian and F. Wang, *Macromolecules*, 2012, **45**, 8412–8419; (f) L.-Y. Niu, Y.-S. Guan, Y.-Z. Chen, L.-Z. Wu, C.-H. Tung and Q.-Z. Yang, *J. Am. Chem. Soc*., 2012, **134**, 18928–18931; (g) H. Zhang, Q. Liu, J. Li and D.-H. Qu, *Org. Lett*., 2013, **15**, 338–341; (h) G.-Z. Zhao, L.-J. Chen, W. Wang, J. Zhang, G. Yang, D.-X. Wang, Y. Yu and H.-B. Yang, *Chem. Eur. J*., 2013, **19**, 10094–10100; (i) X. Yan, D. Xu, J. Chen, M. Zhang, B. Hu, Y. Yu and F. Huang, *Polym. Chem*., 2013, **4**, 3312–3322; (j) B. Xia, B. Zheng, C. Han, S. Dong, M. Zhang, B. Hu, Y. Yu and F. Huang, *Polym. Chem*., 2013, **4**, 2019–2024.

3 (a) H. Tian, B. Qin, R. Yao, X. Zhao and S. Yang, *Adv. Mater*., 2003, **15**, 2104−2107; (b) Y. Wang, N. Ma, Z. Wang and X. Zhang, *Angew. Chem. Int. Ed*., 2007, **46**, 2823–2826; (c) S. Silvi, A. Arduini, A. Pochini, A. Secchi, M. Tomasulo, F. M. Raymo, M. Baroncini and A. Credi, *J. Am. Chem. Soc*., 2007, **129**, 13378–13379; (d) J. Babin, M. Pelletier, M. Lepage, J.-F. Allard, D. Morris and Y. Zhao, *Angew. Chem. Int. Ed*., 2009, **48**, 3329–3332; (e) Q. Yan, J. Yuan, Z. Cai, Y. Xin, Y. Kang and Y. Yin, *J. Am. Chem. Soc*., 2010, **132**, 9268–9270; (f) X. Yan, S. Li, T. R. Cook, X. Ji, Y. Yao, J. B. Pollock, Y. Shi, G. Yu, J. Li, F. Huang and P. J. Stang, *J. Am. Chem. Soc*., 2013, **135**, 14036−14039; (g) X. Yan, B. Jiang, T. R. Cook, Y. Zhang, J. Li, Y. Yu, F. Huang, H.-B. Yang and P. J. Stang, *J. Am. Chem. Soc*., 2013, **135**, 16813−16816.

4 (a) C. Park, H. Kim, S. Kim and C. Kim, *J. Am. Chem. Soc.*, 2009, **131**, 16614–16615; (b) H. Koo, M. S. Huh, I.-C. Sun, S. H. Yuk, K. Choi, K. Kim and I. C. Kwon, *Acc. Chem. Res.*, 2011, **44**, 1018–1028; (c) X. Huang, D. Appelhans, P. Formanek, F. Simon and B. Voit, *ACS Nano*, 2012, **6**, 9718–9726; (d) J. Zhuang, M. R. Gordon, J. Ventura, L. Li and S. Thayumanavan, *Chem. Soc. Rev*., 2013, **42**, 7421−7435; (e) A. R. Rodriguez, J. R. Kramer and T. J. Deming, *Biomacromolecules*, 2013, **14**, 3610−3614.

5 (a) V. Parikh, R. Kozak, V. Martinez and M. Sarter, *Neuron*, 2007, **56**, 141–154; (b) E. Eggermanna and D. Feldmeyer, *Proc. Natl. Acad. Sci. U.S.A*., 2009, **106**, 11753–11758; (c) D.-S. Guo, V. D. Uzunova, X. Su, Y. Liu and W. M. Nau *Chem. Sci.*, 2011, **2**, 1722–1734; (d) Y. Xing, C. Wang, P. Han, Z. Wang and X. Zhang, *Langmuir*, 2012, **28**, 6032−6036; (e) D.-S. Guo, T.-X. Zhang, Y.-X. Wang and Y. Liu, *Chem. Commun*., 2013, **49**, 6779−6781; (f) Y.-L. Sun, Y. Zhou, Q.-L. Li and Y.-W. Yang, *Chem. Commun*., 2013, **49**,

9033−9035; (g) D.-S. Guo, J. Yang and Y. Liu, *Chem. Eur. J*., 2013, **19**, 8755–8759.

6 (a) T. Ogoshi, Y. Nishida, T. Yamagishi and Y. Nakamoto, *Macromolecules*, 2010, **43**, 7068–7072; (b) Z. Zhang, B. Xia, C. Han, Y. Yu and F. Huang, *Org. Lett*., 2010, **12**, 2385–2387; (c) C. Li, L. Zhao, J. Li, X. Ding, S. Chen, Q. Zhang, Y. Yu and X. Jia, *Chem. Commun*., 2010, **46**, 9016–9018; (d) W. Si, X.-B. Hu, X.-H. Liu, R. Fan, Z. Chen, L. Weng and J.-L. Hou, *Tetrahedron Lett*., 2011, **52**, 2484–2487; (e) Y. Yao, M. Xue, J. Chen, M. Zhang and F. Huang, *J. Am. Chem. Soc*., 2012, **134**, 15712−15715; (f) Z. Zhang, C. Han, G. Yu and F. Huang, *Chem. Sci*., 2012, **3**, 3026−3031; (g) P. J. Cragg and K. Sharma, *Chem. Soc. Rev.*, 2012, **41**, 597–607; (h) H. Deng, X. Shu, X. Hu, J. Li, X. Jia and C. Li, *Tetrahedron Lett*., 2012, **53**, 4609–4612; (i) Y. Fang, L. Wu, J. Liao, L. Chen, Y. Yang, N. Liu, L. He, S. Zou, W. Feng and L. Yuan, *RSC Adv*., 2013, **3**, 12376–12383; (j) H. Li, D.-X. Chen, Y.-L. Sun, Y. Zheng, L.-L. Tan, P. S. Weissv Y.-W. Yang, *J. Am. Chem. Soc.*, 2013, **135**, 1570–1576; (k) H. Zhang, K. T. Nguyen, X. Ma, H. Yan, J. Guo, L. Zhu and Y. Zhao, *Org. Biomol. Chem.*, 2013, **11**, 2070–2074; (l) T. Ogoshi and T. A. Yamagishi, *Eur. J. Org. Chem.*, 2013, 2961–2975; (m) J.-F. Xu, Y.-Z. Chen, L.-Z. Wu, C.-H. Tung and Q.-Z. Yang, *Org. Lett*., 2013, **15,** 6148–6151; (n) Y. Ma, M. Xue, Z. Zhang, X. Chi and F. Huang, *Tetrahedron*, 2013, **69**, 4532–4535; (o) C. Li, J. Ma, L. Zhao, Y. Zhang, Y. Yu, X. Shu, J. Li and X. Jia *Chem. Commun.*, 2013, **49**, 1924–1926; (p) S. Dong, J. Yuan and F. Huang, *Chem. Sci*., 2014, **5**, 247–252.

7 (a) D. Cao, Y. Kou, J. Liang, Z. Chen, L. Wang and H. Meier, *Angew. Chem. Int. Ed*., 2009, **48**, 9721–9723; (b) C. Han, F. Ma, Z. Zhang, B. Xia, Y. Yu and F. Huang, *Org. Lett.*, 2010, **12**, 4360–4363; (c) M. Xue, Y. Yang, X. Chi, Z. Zhang and F. Huang, *Acc. Chem. Res*., 2012, **45**, 1294–1308; (d) G. Yu, X. Zhou, Z. Zhang, C. Han, Z. Mao, C. Gao and F. Huang, *J. Am. Chem. Soc*., 2012, **134**, 19489–19497; (e) Y. Ma, X. Chi, X. Yan, J. Liu, Y. Yao, W. Chen, F. Huang and J.-L. Hou, *Org. Lett.*, 2012, **14**, 1532–1535; (f) W. Chen, Y. Zhang, J. Li, X. Lou, Y. Yu, X. Jia and C. Li, *Chem. Comm*., 2013, **49**, 7956–7958; (g) I. Nierengarten, S. Guerra, M. Holler, L. Karmazin-Brelot, J. Barberá, R. Deschenaux and J.-F. Nierengarten, *Eur. J. Org. Chem.*, 2013, 3675–3684. (h) C. Han, L. Gao, G. Yu, Z. Zhang, S. Dong and F. Huang, *Eur. J. Org. Chem*., 2013, 2529–2532; (i) X. Chi, M. Xue, Y. Ma, X. Yan and F. Huang, *Chem. Commun*., 2013, **49**, 8175–8177.

8 (a) J. Terao, A. Tang, J. J. Michels, A. Krivokapic and H. L. Anderson, *Chem. Commun.*, 2004, 56–57; (b) Q.-C. Wang, D.-H. Qu, J. Ren, K. Chen and H. Tian, *Angew. Chem. Int. Ed.*, 2004, **43**, 2661–2665; (c) Y. J. Jeon, H. Kim, S. Jon, N. Selvapalam, D. H. Seo, I. Oh, C.-S. Park, S. Jung, R. D.-S. Koh and K. Kim, *J. Am. Chem. Soc.*, 2004, **126**, 15944–15945; (d) W.-H. Huang, P. Y. Zavalij and L. Isaacs, *Angew. Chem. Int. Ed.*, 2007, **46**, 7425–7427; (e) Y. Liu, A. Bruneau, J. He and Z. Abliz, *Org. Lett.*, 2008, **10**, 765–768; (f) F. Wang, C. Han, C. He, Q. Zhou, J. Zhang, C. Wang, N. Li and F. Huang, *J. Am. Chem. Soc.*, 2008, **130**, 11254-11255; (g) Z. Niu and H. W. Gibson, *Chem. Rev*., 2009, **109**, 6024–6046; (h) W. Jiang, A. Schäfer, P. C. Mohr and C. A. Schalley, *J. Am. Chem. Soc.*, 2010, **132**, 2309–2320; (i) F. Wang, J. Zhang, X. Ding, S. Dong, M. Liu, B. Zheng, S. Li, K. Zhu, L. Wu, Y. Yu, H. W. Gibson and F. Huang, *Angew. Chem., Int. Ed.*, 2010, **49**, 1090-1094; (j) Z. Niu, F. Huang and H. W. Gibson, *J. Am. Chem. Soc.*, 2011, **133**, 2836–2839; (k) K. Zhu, V. N. Vukotic and S. J. Loeb, *Angew. Chem. Int. Ed.*, 2012, **51**, 2168–2172; (l) D.-S. Guo and Y. Liu, *Chem. Soc. Rev.*, 2012, **41**, 5907–5921; (m) Z. Qi, P. M. Molina, W. Jiang, Q. Wang, K. Nowosinski, A. Schulz, M. Gradzielski and C. A. Schalley, *Chem. Sci.*, 2012, **3**, 2073–2082; (n) B. Zheng, F. Wang, S. Dong and F. Huang, *Chem. Soc. Rev.*, 2012, **41**, 1621–1636; (o) Y. Lan, X. J. Loh, J. Geng, Z. Walsh and O. A. Scherman, *Chem. Commun.*, 2012, **48**, 8757–8759; (p) B. Vinciguerra, L. Cao, J. R. Cannon, P. Y. Zavalij, C. Fenselau and L. Isaacs, *J. Am. Chem. Soc.*, 2012, **134**, 13133−13140; (q) X. Yan, F. Wang, B. Zheng and F. Huang, *Chem. Soc. Rev*., 2012, **41**, 6042–6065; (r) D.-S. Guo, K. Wang, Y.-X. Wang and Y. Liu, *J. Am. Chem. Soc.*, 2012, **134**, 10244–10250; (s) Q. Zhang, D.-H. Qu, J. Wu, X. Ma, Q. Wang and H. Tian, *Langmuir*, 2013, **29**, 5345−5350.

9 (a) J.-M. Liu, J.-H. Bu, Q.-Y. Zheng, C.-F. Chen and Z.-T. Huang, *Tetrahedron Lett*., 2006, **47**, 1905–1908; (b) S. Li, J. Chen, B. Zheng, S. Dong, Z. Ma, H. W. Gibson and F. Huang, *J. Polym. Sci. Pol. Chem.*, 2010, **48**, 4067–4073; (c) J. Cao, Z.-P. Song, X.-Z. Zhu and C.-F. Chen, *Tetrahedron Lett*., 2010, **51**, 3112–3115; (d) S. Dong, Y. Luo, X. Yan, B. Zheng, X. Ding, Y. Yu, Z. Ma, Q. Zhao and F. Huang, *Angew. Chem., Int. Ed.*, 2011, **50**, 1905–1909; (e) M. Zhang, D. Xu, X. Yan, J. Chen, S. Dong, B. Zheng and F. Huang, *Angew. Chem., Int. Ed.*, 2012, **51**, 7011–7015; (f) S. Pan, D.-X. Wang, L. Zhao and M.-X. Wang, *Tetrahedron*, 2012, **68**, 9464–9477; (g) Y.-K. Tian, L. Chen, Y.-J. Tian, X.-Y. Wang and F. Wang, *Polym. Chem*., 2013, **4**, 453−457; (h) X. Ji, Y. Yao, J. Li, X. Yan and F. Huang, *J. Am. Chem. Soc.*, 2013, **135**, 74–77; (i) X. Ji, S. Dong, P. Wei, D. Xia and F. Huang, *Adv. Mater.*, 2013, **25**, 5725–5729.

10 (a) Z. Zhang, G. Yu, C. Han, J. Liu, X. Ding, Y. Yu and F. Huang, *Org. Lett*., 2011, **13**, 4818–4821; (b) L. Liu, L. Wang, C. Liu, Z. Fu, H. Meier and D. Cao, *J. Org. Chem*., 2012, **77**, 9413–9417.

11 (a) N. L. Strutt, R. S. Forgan, J. M. Spruell, Y. Y. Botros and J. F. Stoddart, *J. Am. Chem. Soc*., 2011, **133**, 5668–5671; (b) G. Yu, Z. Zhang, C. Han, M. Xue, Q. Zhou and F. Huang, *Chem. Comm*., 2012, **48**, 2958–2960.

12 (a) Z. Zhang, Y. Luo, J. Chen, S. Dong, Y. Yu, Z. Ma and F. Huang, *Angew. Chem. Int. Ed*., 2011, **50**, 1397–1401; (b) Y. Guan, M. Ni, X. Hu, T. Xiao, S. Xiong, C. Lin and L. Wang, *Chem. Commun*., 2012, **48**, 8532–8534; (c) X. Wang, K. Han, J. Li, X. Jia and C. Li, *Polym. Chem*., 2013, **4**, 3998–4003. (e) X.-Y. Hu, X. Wu, S. Wang, D. Chen, W. Xia, C. Lin, Y. Pan and L. Wang, *Polym. Chem*., 2013, **4**, 4292–4297.

13 (a) W. Si, L. Chen, X.-B. Hu, G. Tang, Z. Chen, J.-L. Hou and Z.-T. Li, *Angew. Chem. Int. Ed*., 2011, **50**, 12564–12568; (b) X.-B. Hu, Z. Chen, G. Tang, J.-L. Hou and Z.-T. Li, *J. Am. Chem. Soc.*, 2012, **134**, 8384−8387; (c) L. Chen, W. Si, L. Zhang, G. Tang, Z.-T. Li and J.-L. Hou, *J. Am. Chem. Soc.*, 2013, **135**, 2152−2155.

14 (a) Q. Duan, Y. Cao, Y. Li, X. Hu, T. Xiao, C. Lin, Y. Pan and L. Wang, *J. Am. Chem. Soc*., 2013, **135**, 10542–10549; (b) H. Zhang, X. Ma, K. T. Nguyen and Y. Zhao, *ACS Nano*, 2013, **7**, 7853–7863.

15 G. Yu, Y. Ma, C. Han, Y. Yao, G. Tang, Z. Mao, C. Gao and F. Huang, *J. Am. Chem. Soc*., 2013, **135**, 10310–10313.

16 (a) T. Ogoshi, R. Shiga and T. Yamagishi, *J. Am. Chem. Soc.*, 2012, ***134***, 4577–4580; (b) G. Yu, C. Han, Z. Zhang, J. Chen,

X. Yan, B. Zheng, S. Liu and F. Huang, *J. Am. Chem. Soc*., 2012, **134**, 8711–8717; (c) G. Yu, M. Xue, Z. Zhang, J. Li, C. Han and F. Huang, *J. Am. Chem. Soc*., 2012, **134**, 13248–13251; (d) T. Ogoshi, K. Kida and T. Yamagishi, *J. Am. Chem. Soc*., 2012, **134**, 20146–20150; (e) W. Xia, X.-Y. Hu, Y. Chen, C. Lin and L. Wang, *Chem. Commun*., 2013, **49**, 5085–5087.

17 (a) B.-Y. Lu, G.-J. Sun, J.-B. Lin, X.-K. Jiang, X. Zhao and Z.-T. Li, *Tetrahedron Lett*., 2010, **51**, 3830–3835; (b) Z.-G. Tao, X. Zhao, X.-K. Jiang and Z.-T. Li, *Tetrahedron Lett*., 2012, **53**, 1840–1842; (c) X. Yan, D. Xu, X. Chi, J. Chen, S. Dong, X. Ding, Y. Yu and F. Huang, *Adv. Mater.*, 2012, **24**, 362−369; (d) X. Yan, S. Li, J. B. Pollock, T. R. Cook, J. Chen, Y. Zhang, X. Ji, Y. Yu, F. Huang and P. J. Stang, *Proc. Natl. Acad. Sci. U. S. A*., 2013, **110**, 15585–15590; (e) F. Wang, M. Gillissen, P. J. M. Stals, A. R. A. Palmans and E. W. Meijer, *Chem. Eur. J*., 2012, **18**, 11761–11770; (f) S. Dong, B. Zheng, D. Xu, X. Yan, M. Zhang and F. Huang, *Adv. Mater.*, 2012, **24**, 3191-3195; (g) X. Ji, J. Li, J. Chen, X. Chi, K. Zhu, X. Yan, M. Zhang and F. Huang, *Macromolecules*, 2012, **45**, 6457-6463; (h) T.-Y. Zhou, F. Lin, Z.-T. Li and X. Zhao, *Macromolecules*, 2013, **46**, 7745−7752.

18 (a) K. Liu, Y. Yao, Y. Liu, C. Wang, Z. Li and X. Zhang, *Langmuir*, 2012, **28**, 10697−10702; (b) K. Liu, Y. Yao, C. Wang, Y. Liu, Z. Li and X. Zhang, *Chem. Eur. J*., 2012, **18**, 8622–8628.

19 (a) Y. Yao, M. Xue, X. Chi, Y. Ma, J. He, Z. Ablizb and F. Huang, *Chem. Commun*., 2012, **48**, 6505–6507; (b) Y. Yao, M. Xue, Z. Zhang, M. Zhang, Y. Wang and F. Huang, *Chem. Sci*., 2013, **4**, 3667–3672.